Available online at www.sciencedirect.com
SCIENCE DIRECT®
Journal of Sound and Vibration 273 (2004) 777–792
JOURNAL OF SOUND AND VIBRATION
www.elsevier.com/locate/jsvi

Study of a folded resonator including the effects of higher order modes

R. Glav[a], P.-L. Regaud[b], M. Åbom[b,*]

[a] *Vehicle Acoustics, Scania, S-151 82 Södertälje, Sweden*
[b] *The Marcus Wallenberg Laboratory, KTH, S-100 44 Stockholm, Sweden*

Received 12 July 2002; accepted 9 May 2003

Abstract

This paper presents a derivation of the 2-port matrix for a folded quarter-wave side-branch resonator including higher order modes but neglecting flow interaction effects. The model is restricted to coaxial geometries and two-folds. The derivation is based on the mode matching technique and is verified by measurements done on prototypes. A notable result from these experiments is the effects of a slit-like leakage close to a rigid wall. A parametrical study finally investigates the influence of various lengths and area ratios of the resonator resulting in a set of design rules.

1. Introduction

Duct or pipe systems carrying low-frequency tonal noise are encountered in various applications, such as intake and exhaust systems of vehicles and ventilation systems. To fulfil regulations and comfort requirements, it is of interest to reduce these tones without increasing the pressure drop. A standard solution to this problem is to add various kinds of side-branch resonators such as the Helmholtz or the quarter-wave resonator. The former, being non-harmonic, is mainly aimed at the fundamental frequency while the latter can handle also the odd harmonics. A drawback of the quarter-wave resonator is its bulkiness; to attenuate a fundamental of 100 Hz at room temperature a length of 0.85 m is required. One way to reduce the outer dimensions is to fold the cavity as shown in Fig. 1.

A key issue in the study of resonators is the accurate determination of resonance frequencies. Although, most resonators are used for low-frequency sounds and can be modelled using lumped

*Corresponding author. Tel.: +46-8-790-7944; fax: +46-8-790-6122.
E-mail address: matsabom@kth.se (M. Åbom).

0022-460X/$ - see front matter
doi:10.1016/j.jsv.2003.05.024

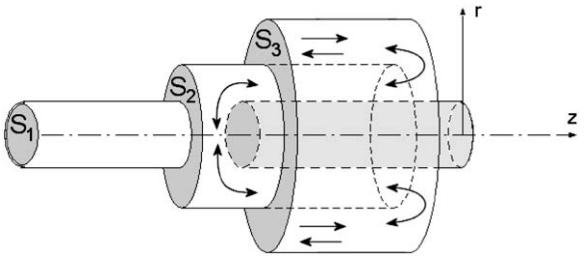

Fig. 1. Folded resonator with the acoustic transmission path indicated by arrows. The co-ordinate system as well as the cross-sectional areas referred to are illustrated.

elements and plane wave fields, effects of non-propagating modes (or near fields) at openings or area discontinuities are important. Often the nearfield effects are included using the so-called end-corrections, which for instance for the case of Helmholtz resonators has been studied extensively.

The folded resonator was suggested by Cummings already in the mid-1970s [1] but a more systematic study of the effects of the folding, in particular, its effect on the resonance frequencies, has not yet been presented. Cummings limited the analysis to two higher order modes and one geometrical configuration. The present paper focuses on geometries of interest for exhaust system applications and presents a model with an unlimited number of higher order modes validated by measurements. Furthermore, the 2-port for a folded resonator is derived, a result most useful for implementation in software dedicated to the analysis of sound in duct networks.

2. Theory

The folded quarter-wave resonator studied here consists of cylindrical pipes of circular or annular cross-section, see Fig. 1. First, analytical expressions in terms of modal expansions for the acoustic pressure and velocity in such ducts will be given. With these stated, straightforward mode-matching will give the acoustic field throughout the device.

2.1. Wave equation

The study is restricted to small perturbations and neglects mean flow and visco-thermal effects. By restricting the analysis to incident plane waves and concentric geometries, as illustrated in Fig. 1, the problem is rotationally symmetric and there is thus no angular dependence. These assumptions yield the wave equation

$$\frac{\partial^2 p}{\partial r^2}+\frac{1}{r}\frac{\partial p}{\partial r}+\frac{\partial^2 p}{\partial z^2}-\frac{1}{c^2}\frac{\partial^2 p}{\partial t^2}=0, \tag{1}$$

where $p(r,z,t)$ is the acoustic pressure inside the pipe and c the speed of sound. The frequency domain solution $P=\int_{-\infty}^{\infty} p(r,z,t)\exp(\mathrm{i}\omega t)\,\mathrm{d}t$ to the wave equation in circular and annular ducts with hard walls is well known. Using the cross-sectional eigenfunctions ψ_n,

$$\psi_n(r,k_{r,n})=\mathrm{J}_0(k_{r,n}r)-(1-\delta_{k_{r,n}r_{\min},0})\frac{\mathrm{J}_1(k_{r,n}a)}{\mathrm{N}_1(k_{r,n}a)}\mathrm{N}_0(k_{r,n}r),\quad n=0,1,\ldots \tag{2}$$

it can be expressed as a sum of propagating modes:

$$P(r,z,\omega)=\sum_n \psi_n[A_n e^{ik_{z,n}z}+B_n e^{-ik_{z,n}z}], \tag{3}$$

where J_m and N_m are the Bessel and Neumann functions of order m ($m=0$ or 1), A_n along with B_n are the wave amplitudes for propagation in positive and negative direction, respectively, $k_{r,n}$ is the radial wave number (or eigenvalue) determined by the hard wall boundary condition and $k_{z,n}$ is the axial wave number. For a circular cross-section, a is the radius and for an annular it is the inner radius, see Fig. 1. The Kronecker symbol $\delta_{k_{r,n}r_{\min},0}$ is equal to unity when either $k_{r,n}$ or the minimum radius vanishes. The corresponding axial particle velocity can as usual be obtained from the momentum equation:

$$U(r,z,\omega)=\sum_n \frac{k_{z,n}}{\omega\rho}\psi_n[A_n e^{ik_{z,n}z}-B_n e^{-ik_{z,n}z}], \tag{4}$$

where ρ is the fluid density.

2.2. Partial fields

Based on Fig. 2 it is clear that the interior of the studied resonator may be divided into six regions, consisting of either circular or annular ducts and where the velocity and pressure fields can be expressed using Eqs. (3) and (4).

With the above expansions of acoustic pressure and velocity, the problem reduces to solving a system of linear equations for a set of unknown wave amplitudes. Equations needed to solve these unknowns are produced by the coupling conditions requiring the pressure and axial velocity to be continuous across each interface between adjacent regions. Additional relations originate from the hard wall boundary, imposing vanishing axial velocity at position $z=0$, l_3 and l_4, respectively. Obviously, the modal expansions need to be truncated. Here for practical reasons, it is performed equally for all regions, thus restricting the number of terms in each sum to N, an approach that will violate the edge condition [2]. In short, this condition, which will secure a unique solution, prescribes the truncated terms to be of the same magnitude in each zone. For a circular expansion, the edge condition can be shown [3] to require that the ratio between the number of modes on

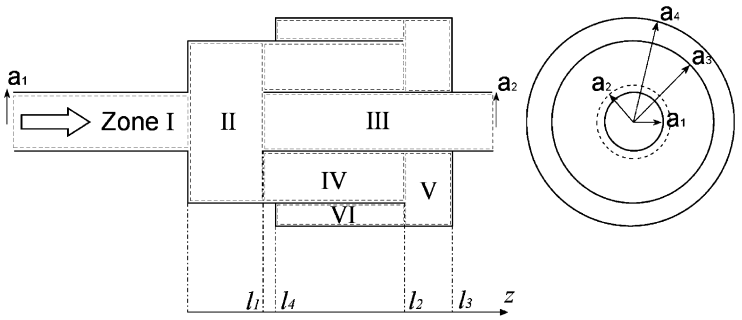

Fig. 2. Lateral and front view of the folded resonator. The areas defined in Fig. 1 are given by $S_1=\pi a_1^2$, $S_2=\pi(a_3^2-a_1^2)$ and $S_3=\pi(a_4^2-a_3^2)$. While the theory presented is general all the cases treated assume that the radius of the inlet and outlet pipes (I and III) are equal.

each side of the expansion equals the radius ratio, i.e., $N_1/N_1 = a_1/a_2$. Even though this condition is not strictly used here, the good agreement with experiments justifies the current approach. A further motivation for this truncation is that most practical applications will require a design with a radius ratio not too far from unity. In addition, and perhaps most importantly, the edge condition is not crucial for the low-frequency plane wave range studied here. It is mainly important for a correct high-frequency (asymptotic) behaviour [4].

With ψ_n^N denoting the eigenfunction of order n in region N, as readily formulated from Eq. (2), the following scalar product may be defined:

$$\langle \psi_n^N | \psi_m^M \rangle_{a_1,a_2} = \int_{a_1}^{a_2} \psi_n^N(r)\psi_m^M(r) r \, \mathrm{d}r, \tag{5}$$

where $[a_1, a_2]$ constitutes the largest interval upon which both functions exist. It can be shown that the eigenfunctions of a given region are orthogonal with respect to this product [5]. Eigenfunctions belonging to different regions are not orthogonal and the integral will then be a measure of the coupling between modes at an interface.

In formulating the acoustic field in each region, it is assumed that solely plane waves can be incident from infinity to regions I and III. This assumption is often satisfied in practice; consider, for instance, the exhaust system of a car where the plane wave range covers the frequency range of interest. Using the preceding notations, the pressure field in each domain can now be written as

$$P^{\mathrm{I}} = A_0^{\mathrm{I}}\psi_0^{\mathrm{I}} \mathrm{e}^{\mathrm{i}k_{z,0}^{\mathrm{I}} z} + \sum_{n=0}^{N} B_n^{\mathrm{I}}\psi_n^{\mathrm{I}} \mathrm{e}^{-\mathrm{i}k_{z,n}^{\mathrm{I}} z}, \tag{6}$$

$$P^{\mathrm{II}} = \sum_{n=0}^{N} [A_n^{\mathrm{II}}\psi_n^{\mathrm{II}} \mathrm{e}^{\mathrm{i}k_{z,n}^{\mathrm{II}} z} + B_n^{\mathrm{II}}\psi_n^{\mathrm{II}} \mathrm{e}^{-\mathrm{i}k_{z,n}^{\mathrm{II}}(z-l_1)}], \tag{7}$$

$$P^{\mathrm{III}} = B_0^{\mathrm{III}}\psi_0^{\mathrm{III}} \mathrm{e}^{-\mathrm{i}k_{z,0}^{\mathrm{III}}(z-l_1)} + \sum_{n=0}^{N} A_n^{\mathrm{III}}\psi_n^{\mathrm{III}} \mathrm{e}^{\mathrm{i}k_{z,n}^{\mathrm{III}}(z-l_1)}, \tag{8}$$

$$P^{\mathrm{IV}} = \sum_{n=0}^{N} [A_n^{\mathrm{IV}}\psi_n^{\mathrm{IV}} \mathrm{e}^{\mathrm{i}k_{z,n}^{\mathrm{IV}}(z-l_1)} + B_n^{\mathrm{IV}}\psi_n^{\mathrm{IV}} \mathrm{e}^{-\mathrm{i}k_{z,n}^{\mathrm{IV}}(z-l_2)}], \tag{9}$$

$$P^{\mathrm{V}} = \sum_{n=0}^{N} [A_n^{\mathrm{V}}\psi_n^{\mathrm{V}} \mathrm{e}^{\mathrm{i}k_{z,n}^{\mathrm{V}}(z-l_2)} + B_n^{\mathrm{V}}\psi_n^{\mathrm{V}} \mathrm{e}^{-\mathrm{i}k_{z,n}^{\mathrm{V}}(z-l_3)}], \tag{10}$$

$$P^{\mathrm{VI}} = \sum_{n=0}^{N} [A_n^{\mathrm{VI}}\psi_n^{\mathrm{VI}} \mathrm{e}^{\mathrm{i}k_{z,n}^{\mathrm{VI}}(z-l_4)} + B_n^{\mathrm{VI}}\psi_n^{\mathrm{VI}} \mathrm{e}^{-\mathrm{i}k_{z,n}^{\mathrm{VI}}(z-l_2)}]. \tag{11}$$

The choice of origin for each of the different modes ensures that the exponential factors are decaying for non-propagating modes, which produces a numerically more robust formulation [6]. The axial velocities can be formulated using the same notation and are thus not explicitly given here.

2.3. Mode matching

This technique implies that the boundary conditions are satisfied in an averaged sense using a Galerkin or integral ("weak") formulation. By utilizing the above-stated orthogonality relations a system of linear equations in the wave amplitudes A_n and B_n can be obtained.

Regions V and VI, each ended by a hard wall at $z = l_3$ and l_4, respectively, will be considered first. Using orthogonality in region VI implies

$$\langle U^{\mathrm{VI}}(z = l_4)|\psi_i^{\mathrm{VI}}\rangle_{a_3,a_4} = A_i^{\mathrm{VI}} - B_i^{\mathrm{VI}}\mathrm{e}^{-\mathrm{i}k_{z,i}^{\mathrm{VI}}(l_4-l_2)} = 0 \tag{12}$$

and thus

$$A_i^{\mathrm{VI}} = B_i^{\mathrm{VI}}\mathrm{e}^{-\mathrm{i}k_{z,i}^{\mathrm{VI}}(l_4-l_2)} \quad \text{for } 0 \leqslant i \leqslant N. \tag{13}$$

Similarly for region V,

$$A_i^{\mathrm{V}} = B_i^{\mathrm{V}}\mathrm{e}^{-\mathrm{i}k_{z,i}^{\mathrm{V}}(l_3-l_2)} \quad \text{for } 0 \leqslant i \leqslant N. \tag{14}$$

As suggested by Eqs. (13) and (14), the amplitudes A_i^{V} and A_i^{VI} can be determined independent of the other domains, reducing the number of unknowns with $2(N + 1)$.

Consider now the intersection between regions II, III and IV at $z = l_1$. The mode-matching technique can be applied in several ways, which are all equivalent when an infinite number of modes are included. But in practice the mode sums will be truncated and different mode matching strategies are no longer equivalent. As suggested for instance by Åbom [6], it is convenient to choose a formulation that reduces to the established plane wave solution, i.e., continuity of pressure and volume velocity, in the case of no higher order modes. This can be achieved by using the orthogonality relations for regions III and IV when matching pressure and region II when matching velocity. Thus, applied to the continuity of velocity at $z = l_1$,

$$\langle U^{\mathrm{II}}|\psi_i^{\mathrm{II}}\rangle_{0,a_3} = \langle U^{\mathrm{III}}|\psi_i^{\mathrm{II}}\rangle_{0,a_2} + \langle U^{\mathrm{IV}}|\psi_i^{\mathrm{II}}\rangle_{a_2,a_3}. \tag{15}$$

This gives

$$\begin{aligned}(A_i^{\mathrm{II}}\mathrm{e}^{k_{z,i}^{\mathrm{II}}l_1} - B_i^{\mathrm{II}})\frac{k_{z,i}^{\mathrm{II}}}{\omega\rho}\int_0^{a_3}(\psi_i^{\mathrm{II}})^2 r\,\mathrm{d}r = &-B_0^{\mathrm{III}}\frac{k_{z,0}^{\mathrm{III}}}{\omega\rho}\int_0^{a_2}\psi_0^{\mathrm{III}}\psi_i^{\mathrm{II}} r\,\mathrm{d}r \\ &+\sum_{n=0}^{N}A_n^{\mathrm{III}}\frac{k_{z,n}^{\mathrm{III}}}{\omega\rho}\int_0^{a_2}\psi_n^{\mathrm{III}}\psi_i^{\mathrm{II}} r\,\mathrm{d}r \\ &+\sum_{n=0}^{N}\left[(A_n^{\mathrm{IV}} - B_n^{\mathrm{IV}}\mathrm{e}^{-k_{z,n}^{\mathrm{IV}}(l_1-l_2)})\frac{k_{z,n}^{\mathrm{IV}}}{\omega\rho}\int_{a_2}^{a_3}\psi_n^{\mathrm{IV}}\psi_i^{\mathrm{II}} r\,\mathrm{d}r\right].\end{aligned} \tag{16}$$

Matching the pressure fields of regions II and III,

$$\langle P^{\mathrm{III}}|\psi_i^{\mathrm{III}}\rangle_{0,a_2} = \langle P^{\mathrm{II}}|\psi_i^{\mathrm{III}}\rangle_{0,a_2}, \tag{17}$$

yields

$$\begin{aligned}(A_0^{\mathrm{III}} + B_0^{\mathrm{III}})\textstyle\int_0^{a_2}(\psi_0^{\mathrm{III}})^2 r\,\mathrm{d}r = \sum_{n=0}^{N}(A_n^{\mathrm{II}}\mathrm{e}^{\mathrm{i}k_{z,n}^{\mathrm{II}}l_1} + B_n^{\mathrm{II}})\textstyle\int_0^{a_2}\psi_n^{\mathrm{II}}\psi_0^{\mathrm{III}} r\,\mathrm{d}r \quad \text{for } i = 0, \\ A_i^{\mathrm{III}}\textstyle\int_0^{a_2}(\psi_i^{\mathrm{III}})^2 r\,\mathrm{d}r = \sum_{n=0}^{N}(A_n^{\mathrm{II}}\mathrm{e}^{\mathrm{i}k_{z,n}^{\mathrm{II}}l_1} + B_n^{\mathrm{II}})\textstyle\int_0^{a_2}\psi_n^{\mathrm{II}}\psi_i^{\mathrm{III}} r\,\mathrm{d}r, \quad 0 < i \leqslant N,\end{aligned} \tag{18}$$

Table 1
Mode matching relations

$z=0$	$\langle P^{\mathrm{I}}\|\psi_i^{\mathrm{I}}\rangle_{0,a_1} = \langle P^{\mathrm{II}}\|\psi_i^{\mathrm{I}}\rangle_{0,a_1}$
	$\langle U^{\mathrm{I}}\|\psi_i^{\mathrm{II}}\rangle_{0,a_1} = \langle U^{\mathrm{II}}\|\psi_i^{\mathrm{II}}\rangle_{0,a_3}$
$z=l_1$	$\langle P^{\mathrm{III}}\|\psi_i^{\mathrm{III}}\rangle_{0,a_2} = \langle P^{\mathrm{II}}\|\psi_i^{\mathrm{III}}\rangle_{0,a_2}$
	$\langle P^{\mathrm{IV}}\|\psi_i^{\mathrm{IV}}\rangle_{a_2,a_3} = \langle P^{\mathrm{II}}\|\psi_i^{\mathrm{IV}}\rangle_{a_2,a_3}$
	$\langle U^{\mathrm{III}}\|\psi_i^{\mathrm{II}}\rangle_{0,a_2} + \langle U^{\mathrm{IV}}\|\psi_i^{\mathrm{II}}\rangle_{a_2,a_3} = \langle U^{\mathrm{II}}\|\psi_i^{\mathrm{II}}\rangle_{0,a_3}$
$z=l_2$	$\langle P^{\mathrm{IV}}\|\psi_i^{\mathrm{IV}}\rangle_{a_2,a_3} = \langle P^{\mathrm{V}}\|\psi_i^{\mathrm{IV}}\rangle_{a_2,a_3}$
	$\langle P^{\mathrm{VI}}\|\psi_i^{\mathrm{VI}}\rangle_{a_3,a_4} = \langle P^{\mathrm{V}}\|\psi_i^{\mathrm{VI}}\rangle_{a_3,a_4}$
	$\langle U^{\mathrm{IV}}\|\psi_i^{\mathrm{V}}\rangle_{a_2,a_3} + \langle U^{\mathrm{VI}}\|\psi_i^{\mathrm{V}}\rangle_{a_3,a_4} = \langle U^{\mathrm{V}}\|\psi_i^{\mathrm{V}}\rangle_{a_2,a_4}$

and likewise for region II and IV

$$\langle P^{\mathrm{IV}}|\psi_i^{\mathrm{IV}}\rangle_{a_2,a_3} = \langle P^{\mathrm{II}}|\psi_i^{\mathrm{IV}}\rangle_{a_2,a_3}. \tag{19}$$

We have

$$(A_i^{\mathrm{IV}} + B_i^{\mathrm{IV}} \mathrm{e}^{-\mathrm{i}k_{z,i}^{\mathrm{IV}}(l_1-l_2)}) \int_{a_2}^{a_3} (\psi_i^{\mathrm{IV}})^2 r \,\mathrm{d}r = \sum_{n=0}^{N} (A_n^{\mathrm{II}} \mathrm{e}^{\mathrm{i}k_{z,n}^{\mathrm{II}} l_1} + B_n^{\mathrm{II}}) \int_{a_2}^{a_3} \psi_n^{\mathrm{II}} \psi_i^{\mathrm{IV}} r \,\mathrm{d}r, \quad 0 \leqslant i \leqslant N. \tag{20}$$

As it is straightforward to derive the corresponding relations for the remaining intersections, this is not reported here. The complete set of linear relations resulting from these and the above efforts are most conveniently summarized in Table 1.

2.4. Numerical solution

The system of equations (6)–(11) contains a total of $10N + 12$ modal amplitudes. To obtain a well-defined problem one can [6], e.g., specify the plane wave pressure and velocity at the inlet ($z = 0$, region I) or at the outlet ($z = l_1$, region III). This reduces the number of unknowns to $10N + 10$. Each line in Table 1 results in $N + 1$ equations, i.e., a total of $8N + 8$ equations. Together with the $2N + 2$ relations stemming from Eqs. (13) and (14) a complete system of linear equations results. This system was coded and solved using Matlab routines. The solvability of the system requires the system matrix to be non-singular and preferably to have a "small" condition number to reduce numerical errors. Based on test calculations it was found that the suggested formulation satisfies these requirements. In particular the choice of origin for the modes, as discussed in Section 2.2, is critical to ensure a small condition number.

In this application, it is not of primary interest to solve the entire acoustic field but rather to obtain the 2-port or transfer matrix for a given frequency

$$\begin{bmatrix} P^0_{in} \\ Q^0_{in} \end{bmatrix} = \begin{bmatrix} t_{11} & t_{12} \\ t_{21} & t_{22} \end{bmatrix} \begin{bmatrix} P^0_{out} \\ Q^0_{out} \end{bmatrix}, \tag{21}$$

where P^0, Q^0 stands for the plane wave pressure and volume velocity, respectively, at $z = 0$ in region I (in) and at $z = l_1$ in region III (out). This matrix is most suitably obtained by solving the system for two different loads, typically $\{P^0_{out} = 1,\ \ Q^0_{out} = 0\}$ and $\{P^0_{out} = 0,\ \ Q^0_{out} = 1\}$. From the elements of the transfer matrix it is straightforward to derive the transmission loss of the folded resonator [7],

$$TL = 10\log\left(\frac{1}{4}\frac{Z_{out}(1+M_{out})^2}{Z_{in}(1+M_{in})^2}\left|t_{11} + \frac{t_{12}}{Z_{out}} + Z_{in}t_{21} + \frac{Z_{in}t_{22}}{Z_{out}}\right|^2\right), \tag{22}$$

where Z denotes the wave impedance of the duct and M the Mach number.

3. Measurements

The measurements were performed in the flow acoustic test facility at the Marcus Wallenberg Laboratory using the two-source method to determine the transfer matrix [8]. The measurement technique and equipment are detailed in Ref. [9] and thus not further discussed here. Even though the numerical simulations neglect any influence of mean flow, measurements were realized up to Mach number 0.1 in order to preliminary investigate the effect of grazing flow on the folded resonator.

3.1. The folded resonator

The resonator used in the measurements, shown in Fig. 3, was designed to attenuate low-frequency tonal noise with a fundamental around 70 Hz, i.e., typical for the firing frequency of a truck diesel.

The diameters given in Fig. 3 are outer diameters; the standard plastic pipes used have a wall thickness increasing with the diameter: 3, 5 and 7.2 mm, respectively. To enable variations of the axial dimensions the prototype was equipped with rubber sealing strips instead of being cemented. This flexibility is utilized in additional studies that are not presented here but are reported in

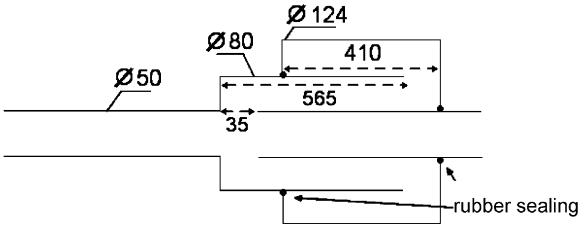

Fig. 3. The folded resonator used in the measurements. All measures are in mm and the outer diameters are specified.

Table 2
Comparison between the calculated and measured attenuation peaks

Resonance	Measured (Hz)	Calculated (Hz)	Difference (Hz)
1st	72	73	−1
2nd	283	287.5	−4.5
3rd	425	432.5	−7.5
4th	639	644	−5
5th	790	805.5	−15.5

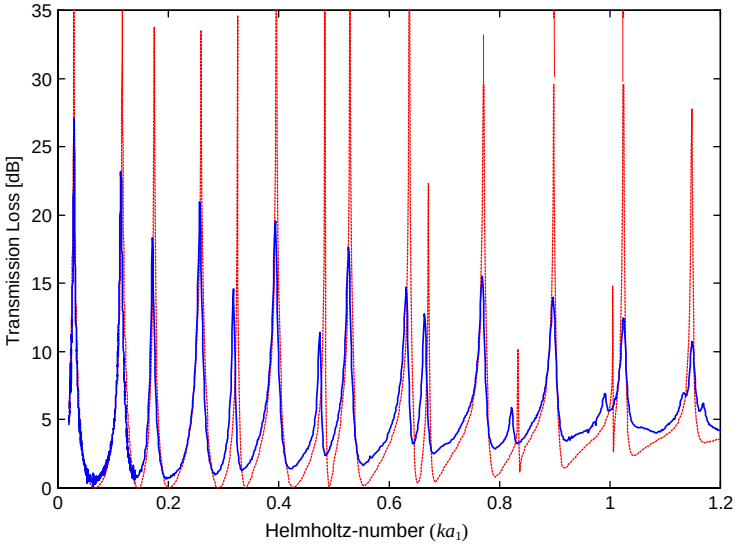

Fig. 4. Transmission loss measurement on a folded resonator; $a_1 = a_2$, $a_3/a_1 = 1.59$, $a_4/a_1 = 2.34$, $l_1/a_1 = 1.59$, $l_2/a_1 = 25.68$, $l_3 = l_2 + l_1$, $l_4/a_1 = 8.63$. Calculated $N = 8$ (- - - -); measured (——). For the geometry, see Figs. 2 and 3.

Ref. [10]. The conclusions of these studies are in agreement with the results presented below. In order to test an arbitrary resonator the area ratio S_3/S_2 (see Fig. 1) used was 1.75, whereas for a true quarter-wave resonator it should equal 1. This area difference generates a distinct non-periodicity that is shown in Table 2 and Fig. 4. Concerning the effects of finite wall thickness in the resonator, this effect was investigated [10] and the best fit to data was found by choosing the radii so that each region corresponds to the air filled space. The frequency range was restricted to the plane wave regime including eight higher order modes to model nearfield effects.

The measurements generally show a good agreement and a deviation of less than 2% at the attenuation peaks (“resonances”). This deviation is relatively constant over the entire frequency range and the calculated values are systematically larger, see Table 2. Yielding walls, reducing the effective speed of sound in the measurements could cause this, the effect of finite wall thickness mentioned above could also have some influence. Another source of systematic errors could of course be a faulty definition of the geometrical length. In this case, however, the precision used to build the resonator rules out this possibility. Table 2 shows that the first five harmonics are

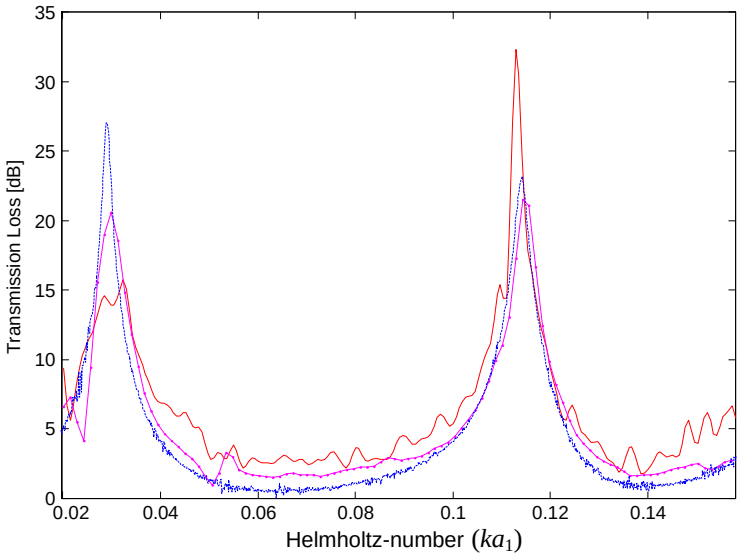

Fig. 5. Influence of the Mach number on the transmission loss of a folded resonator in the low-frequency range. Same case as in Fig. 4. Mach-number = 0 (- - - -); Mach-number = 0.05 (—●—); Mach-number = 0.1 (——).

predicted within a few Hertz. The frequency resolution of the measurement being 0.31 Hz for the first two peaks and 2.5 Hz for higher frequencies. The increase of the simulated minimum attenuation level with frequency is due to the first expansion and would also be present in an analysis restricted to plane waves [10]. At the resonance peaks the measured transmission loss is systematically less than the calculated and at minima the measured levels are higher. These effects are mainly created by the neglect of viscous and thermal losses in the model, which leads to a smoothing of the transmission loss curve. The effect increases with frequency and can also be found in the subsequent measurements.

As indicated above, measurements with flow ranging up to a Mach number of 0.1 were also performed for the current configuration. The objective was to evaluate the transmission loss of the folded silencer in a more realistic case. As no effects of mean flow are included in the simulations Fig. 5 only reports measured values. As expected at low frequencies, flow-induced losses lead to a reduction and widening of the first peak. The results also indicate the tendency of the end-correction (see Section 4.4) to "disappear" with increasing grazing flow, as reported earlier by, e.g., Cummings [11]. This appears in Fig. 5 as a trend for a shift upwards in frequency with increasing Mach number (compare 0 and 0.1).

3.2. A note on leakage

A well-known problem in the practical use of resonators is leakage between the different cavities of the device. This is often encountered, e.g., in automotive silencers where an airtight design is difficult to achieve with conventional manufacturing techniques. A leakage is critical as it may considerably alter, or in the worst case totally ruin, the desired resonant character. This may be illustrated with the resonator used above by rearranging the pipes so that region V almost

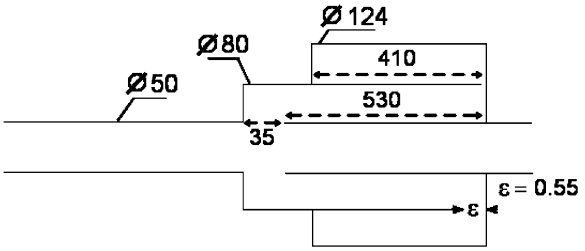

Fig. 6. Lateral cut of the resonator with a slit-like leakage at the end wall. All measures are in mm.

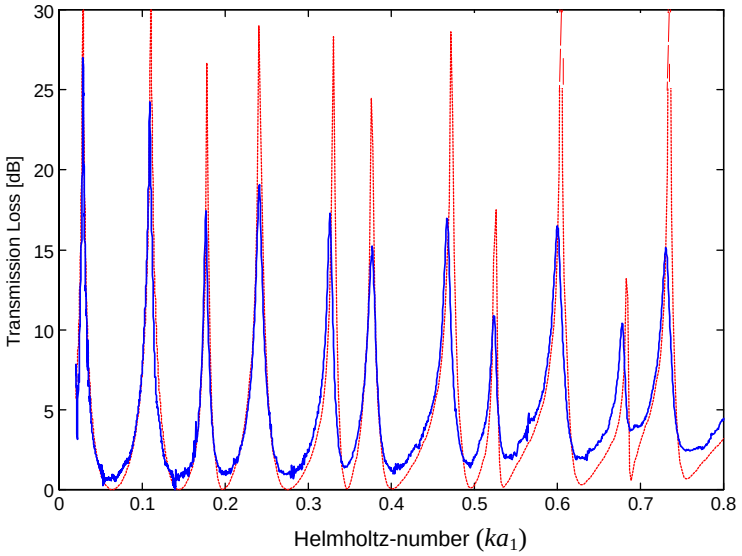

Fig. 7. Transmission loss measurement for the case with leakage; $a_1 = a_2$, $a_3/a_1 = 1.59$, $a_4/a_1 = 2.34$, $l_1/a_1 = 1.59$, $l_2/a_1 = 25.68$, $l_3 = l_2 + \varepsilon$, $l_4/a_1 = 7.045$. Calculated $N = 8$ (- - - -); measured (——). For the geometry, see Figs. 2 and 6.

completely vanishes giving a slit-like leakage of width 0.55 mm in region VI, see Fig. 6. Thus, instead of the desired single folded quarter wave resonator of physical length 530 mm and a harmonic attenuation pattern with peaks at $ka_1 = 0.07, 0.22, 0.37, \ldots$, a double folded non-harmonic device of total length 940 mm with peaks at $ka_1 = 0.03, 0.12, 0.18, \ldots$, is obtained, see Fig. 7.

Apparently the effect of the leakage is quite well captured by the simulation. This may seem surprising since it might be expected that viscous losses would become important for such a narrow slit, with a width comparable to the viscous boundary layer thickness (0.25 mm at the first peak). Since no dramatic viscous losses occur there is apparently negligible fluid motion and thus there is negligible acoustic pressure drop through the leakage. The leakage will therefore act as a "zero" impedance element, which tends to "short circuit" the acoustic wall pressures in the two branches. Obviously this result is connected to the presence of the rigid wall at $z = l_3$.

4. Simulations

The usefulness of a certain resonator design is dependent upon a number of features such as "acoustical length", i.e., which fundamental resonance will be obtained for a given geometry, width of the attenuation peaks and to what extent the resonator has a harmonic character. Here width is defined as the relative bandwidth around a peak frequency where the transmission loss is larger than (say) 20 dB. Below the presented model has been used to investigate the influence of the geometrical parameters, i.e., the length and area of the different regions of the folded resonator, upon these features. The basic dimensions of the resonator used for the simulations are chosen to give a realistic design for exhaust system applications. This gives a slender shape with a first frequency peak matching a typical IC-engine firing frequency (resonator length $20a_1$). All simulations have been performed using eight higher order modes.

4.1. Equal area resonator

To obtain a harmonic character of a folded resonator it seems reasonable to keep the cross-sectional area encountered by the standing wave field constant. In Fig. 8 such an "equal area resonator" is presented and compared to the harmonic pattern of an "ideal" side-branch quarter wave resonator. Clearly, the equal area resonator exhibits an almost perfect harmonic character with a deviation of not more than 1% in the present example. As could be expected from the mass character of the nearfield effects, the largest deviation is obtained for the higher frequencies.

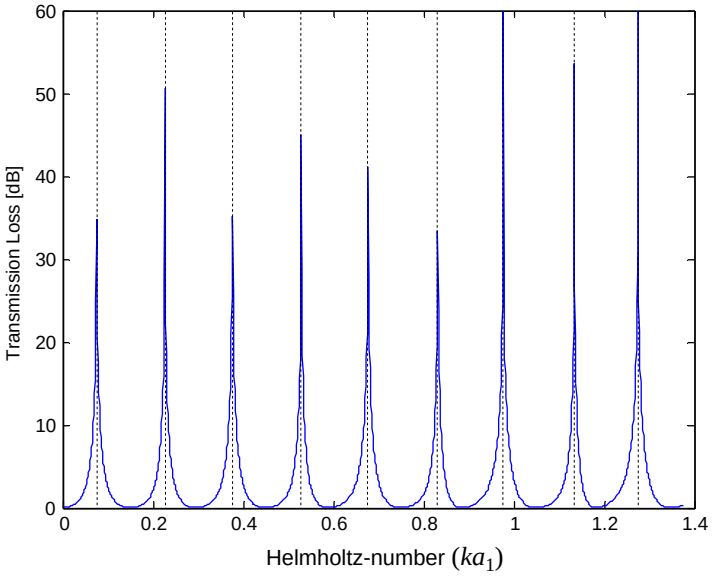

Fig. 8. Simulated transmission loss of a folded equal area resonator; $a_1 = a_2$, $a_3 = \sqrt{2}a_1$, $a_4 = \sqrt{3}a_1$, $l_1 = a_1/2$, $l_2 = l_1 + 10a_1$, $l_3 = l_2 + a_1/\sqrt{8}$, $l_4 = l_1$. Note that the area ratio "resonator to main duct", i.e., $S_2/S_1 = S_3/S_1$ is 1. The vertical lines represent the harmonic pattern of the corresponding ideal quarter wave resonator. For the geometry, see Fig. 2.

The acoustical length of the folded resonator, defined as the length of the corresponding ideal quarter wave resonator matching the first peak, is 4.6% larger than the geometrical length given by the overall length of regions IV and VI ($20a_1$). Deviations from this design will give a non-harmonic character, at least for the higher attenuation peaks. Of course in applications with a restricted number of harmonics such resonators may still be of interest.

4.2. *Effect of inlet width*

Simulations show that changes of the length of the reverse chamber, i.e., region V will break the harmonic pattern obtained above. What remains then is to study the influence of the inlet to the resonator, i.e., the length of region II. Consequently, this has been varied with respect to the equal area resonator specified above. In Fig. 9, the effect of a 10 times elongated inlet section is shown.

Obviously, the harmonic pattern is very much conserved and moreover, the fundamental frequency is unaltered. The larger opening also has a small affect on the width of the attenuation peaks, but introduces an expansion chamber behavior as can be discerned from the figure. It appears that the behavior at the peaks of the folded resonator is controlled by the main body of the resonator and only weakly affected by the inlet section.

To further test this conclusion the inlet width has also been decreased to merely a tenth of the equal area case. The result is shown in Fig. 10 again with the equal area resonator as reference. For this more compact device there is a harmonic character for the first peaks. For higher frequencies there are deviations from the harmonic character with a largest discrepancy of 2.1% for the eighth resonance. It can also be noted that the fundamental frequency is lowered 3.0% with respect to the equal area resonator.

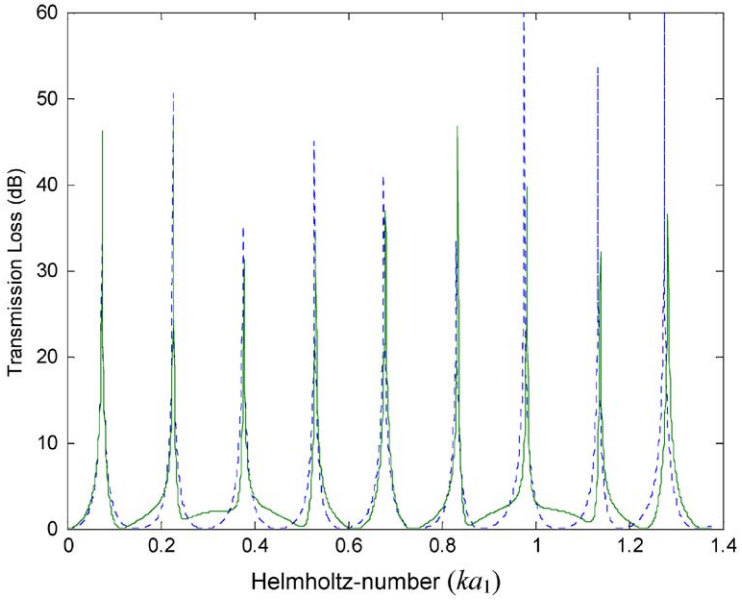

Fig. 9. Simulated transmission loss of a folded resonator with large inlet width; $l_1 = 5a_1$ and the other data as in Fig. 8. The dotted line represents the equal area resonator from Fig. 8.

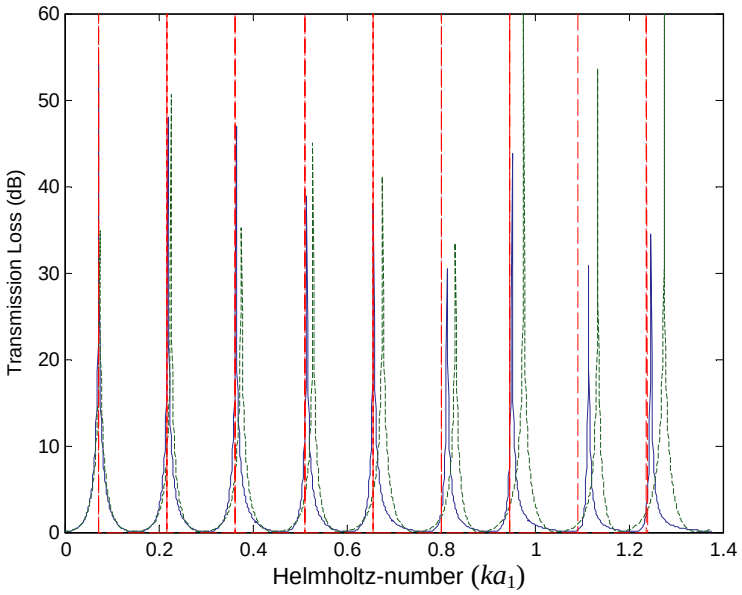

Fig. 10. Simulated transmission loss of a folded resonator with a slit-like inlet; $l_1 = a_1/20$ and the other data as in Fig. 8. The vertical lines represent the harmonic pattern of the corresponding ideal quarter wave resonator. The dotted line represents the equal area resonator from Fig. 8.

This implies that a geometrically more compact resonator acoustically appears to be longer, i.e., to produce a lower fundamental frequency compared to the equal area case. Consequently, the end-correction is increasing with decreasing inlet width in the current example. Considering the peak width it is weakly affected for the lowest peaks but higher up in frequency it is reduced.

4.3. *Area of the folds*

As seen in Section 4.2 the inlet area to the folded resonator typically has a small influence on the attenuation peak width. The width of the peaks is instead controlled by the cross-sectional area of the folds, i.e., is determined by the main body of the resonator. This is illustrated in Fig. 11, where the reference equal area resonator (Section 4.1) is compared to an equal area resonator with five times larger cross-section. Note, omission of the inlet width in this overall increase in area would render a non-harmonic character (for the higher harmonics) as indicated by the results reported above.

As seen from Fig. 11 the desired increase in peak width is obtained without any considerable change in harmonic character. The deviation is less than 1%. Compared to the original equal area resonator the fundamental frequency is lowered 5% implying a larger near field at, as demonstrated in Section 4.4, mainly the reverse chamber (region V).

4.4. *End-corrections*

Before concluding the above observations in some simple design rules the relation between geometrical and acoustical length will be further investigated. The case of the equal area

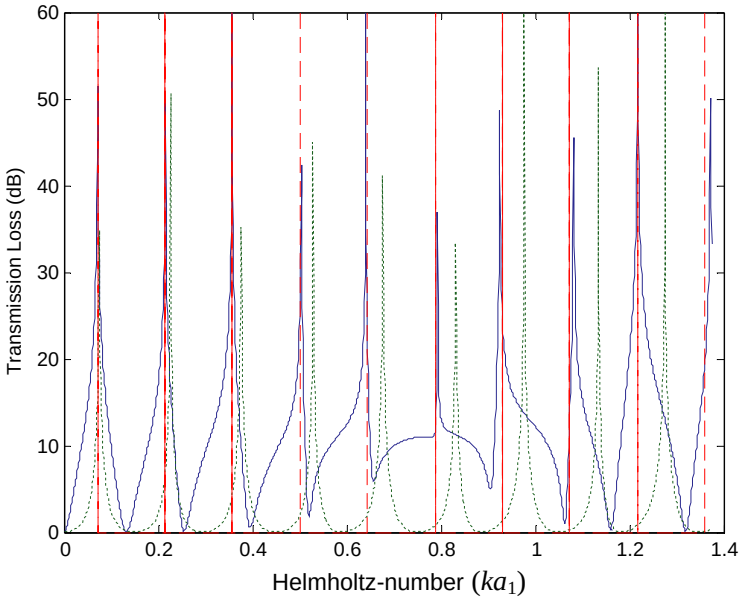

Fig. 11. The simulated transmission loss of an equal area resonator with 5 times larger cross-sectional area; $a_1 = a_2$, $a_3 = \sqrt{6}a_1$, $a_4 = \sqrt{11}a_1$, $l_1 = 5a_1/2$, $l_2 = l_1 + 10a_1$, $l_3 = l_2 + \sqrt{25/24}a_1$ and $l_4 = l_1$, compared to the equal area resonator of Section 4.1 represented by the dotted line. The vertical lines represent the harmonic pattern of the corresponding ideal quarter wave resonator. For the geometry, see Fig. 2.

resonator, which preserves an almost perfect harmonic pattern, will be further analyzed. The difference between the acoustical and geometrical length L of the resonator is normally referred to as the "end-correction" (ΔL). The end-correction captures the inherent mass character of the incompressible field at the inlet (region II) and at the reverse chamber (region V). Using the acoustical length, $L + \Delta L$, the classical rule for the ideal quarter wave resonator applies: *maximum attenuation for frequencies where the length equals odd multiples of one-quarter of the wavelength*. By using the derived model and analyzing resonators with the same length but with one (only inlet ΔL) or two-folds (both inlet and reverse chamber ΔL), it is possible to separate the inlet and reverse chamber end-corrections. Fig. 12 presents the relative end-correction for an equal area resonator of geometrical length L equal to $20a_1$. In the figure the end-correction is split in two parts representing the inlet and the reverse chamber, respectively. The overall obviously being the sum of these two partial corrections. A clear difference in the character between the two curves can be noted. The inlet correction reaches asymptotically a constant value, while the reverse chamber correction is monotonically growing. The reason may be that the upstream pipe dimension, along with the geometrical length of the resonator, are constant. An increase in cross-sectional area of the folds will thus reshape the geometry of the inlet towards something similar to a baffled expansion. The reverse chamber, on the other hand, will instead grow uniformly adding an extra path to the sound wave, thereby increasing the end-correction relative the fixed geometrical length.

Apparently, for most designs envisaged in practice the overall end-correction will be somewhere between 2 and 5%.

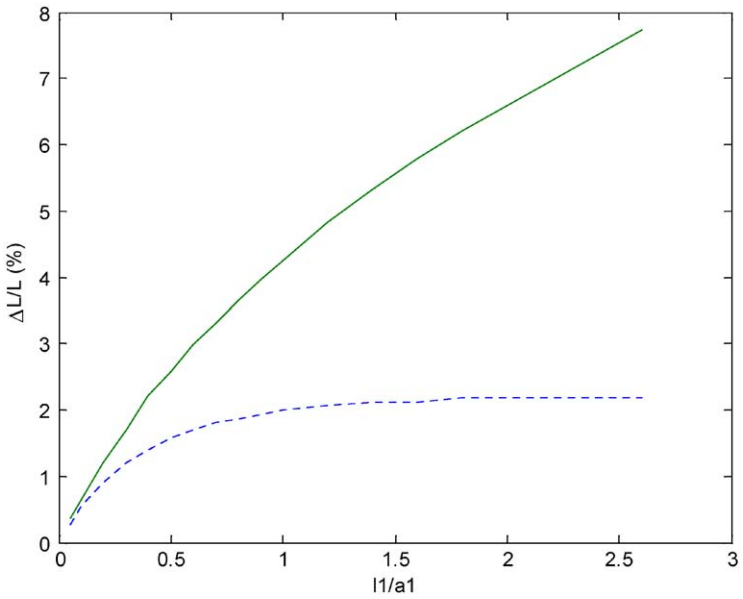

Fig. 12. The relative end-correction of the inlet (dotted line) and of the reverse chamber, respectively, in an equal area resonator; $a_2 = a_1$, $a_3 = a_1\sqrt{(2l_1/a_1 + 1)}$, $a_4 = a_1\sqrt{(4l_1/a_1 + 1)}$, $l_2 = l_1 + 10a_1$, $l_3 = l_1\sqrt{(2l_1/a_1 + 1)} + l_2$, $l_4 = l_1$, as function of the normalized inlet width. Note, $l_1/a_1 = 0.5$ corresponds to an area ratio of 1 between the main pipe and the resonator.

4.5. Design rules

The results presented above along with further simulations not presented here [10] may be summarized in a few simple rules. The rules apply for the type of folded resonator shown in Fig. 1 and for applications in the low-frequency plane wave range.

- To obtain a harmonic peak (“resonance”) pattern the cross-sectional area of the folded side-branch should be constant throughout the device (*equal area resonator*).

This concerns not only the area of the folds S_2 and S_3 but also the annular inlet and reverse sections, i.e., regions II and V with area $2\pi a_1 l_1$ and $2\pi a_3(l_3 - l_2)$, respectively, see Fig. 2.

- The width of the attenuation peaks (“resonances”) are controlled by the area of the folds (S_2 and S_3) relative the main duct (S_1) and are only weakly affected by the area of the inlet or reverse sections.
- Reduction of the inlet width will lower the fundamental resonance compared to the corresponding equal area resonator and not preserve the harmonic character.
- An increased inlet width will not increase the fundamental resonance compared to the corresponding equal area resonator and preserve the harmonic character.

5. Conclusions

A study of a folded side-branch resonator with applications to, e.g., low-frequency tones in exhaust systems has been presented. A derivation of the 2-port matrix for the resonator including higher order modes but neglecting mean flow is included. The result has been coded and is suitable for implementation in software for acoustic plane wave analysis of duct networks, e.g., SID [12]. Being two-dimensional, the derived solution is restricted to coaxial geometries, but otherwise enables modelling of various geometries like for instance an expansion chamber with extended outlet. The model is based on the mode-matching technique and is validated by experiments done on prototypes.

The model has been used to simulate the influence of various geometrical parameters upon harmonic behaviour, peak width and end-corrections. These efforts are summarized in a few rules for the design of folded side-branch resonators. An interesting result concerning leakage was observed both in the simulations and experiments. A leakage (''small opening'') close to a hard wall will act as acoustically transparent. This may be of practical interest as it enables the design of a folded resonator with both a small inlet and a small reverse chamber resulting in a compact resonator. Such a design would not affect the width of the lowest peaks and also produce at least 3–5 peaks that follow a harmonic pattern.

The present study was limited to two-folds but could straightforwardly although tediously be extended to N folds in future works. This would make it possible to search for folded configurations that include all harmonics of a fundamental, e.g., approximating the shape of a conical horn [13]. Another item of interest requiring further investigations are the effects of mean flow, for instance, to what extent flow induced losses could be reduced by using a slit-like inlet.

References

[1] A. Cummings, Sound transmission in a folded annular duct, *Journal of Sound and Vibration* 41 (3) (1975) 375–379.
[2] R. Mitra, W. Lee, *Analytical Techniques in the Theory of Guides Waves,* Macmillan, New York, 1971.
[3] H. Hudde, U. Letens, Scattering matrix of a discontinuity with a nonrigid wall in a lossless circular duct, *Journal of the Acoustical Society of America* 78 (1985) 1826–1837.
[4] B. Nilsson, Växjö University/MSI, SWEDEN, Personal communication.
[5] M. Abramowitz, A. Stegun, *Handbook of Mathematical Functions,* Dover, New York, 1970.
[6] M. Åbom, Derivation of four-pole parameter including higher order mode effects for expansion chamber mufflers with extended inlet and outlet, *Journal of Sound and Vibration* 137 (1990) 403–418.
[7] M.L. Munjal, *Acoustic of Ducts and Mufflers,* Wiley-Interscience, New York, 1987.
[8] M. Åbom, Measurement of the scattering-matrix of acoustical 2-ports, *Mechnical Systems and Signal Processing* 5 (2) (1991) 89–114.
[9] Å. Stenman, Vikta Kvartvågsresonatorer, M.Sc. Thesis, MWL, Royal Institute of Technology, Stockholm, TRITA FKT 01:30, 2001.
[10] P.-L. Regaud, Modelling of Compact Resonators, Lic. Tech thesis, MWL, Royal Institute of Technology, Stockholm, TRITA FKT 01:31, 2001.
[11] A. Cummings, The effect of grazing turbulent pipe-flow on the impedance of an orifice, *Acoustic* 61 (1986) 233–242.
[12] R. Glav, Computer simulation of sound propagation in inlet and exhaust systems, in: *Proceedings ISATA* 92, 1992, pp. 161–167.
[13] J.P. Dalmont, J. Kergomard, Lattices of sound tubes with harmonically related eigenfrequencies, *Acta Acoustic* 2 (1994) 421–430.